Heat Transfer and Solidification Modeling of Continuous Steel Slab Casting

R.A. Hardin[1], C. Beckermann[1]
[1]Department of Mechanical and Industrial Engineering, University of Iowa,
3131Seamans Center, Iowa City, IA, USA, 52242
Phone: (319)335-5681
Email:becker@engineering.uiowa.edu

Keywords: Steel, continuous casting, solidification, simulation, spray cooling, modeling, heat transfer

ABSTRACT

A three-dimensional heat transfer and solidification model for continuous steel casting is presented. It is developed such that simulations for continuous casters having a rectangular mold shape with any configuration of rolls and secondary spray cooling nozzles can be simulated using realistic operating conditions. The heat transfer in the mold, from each roll, to the environment through natural convection and radiation, and due to cooling water spray from individual spray nozzles are modeled. Conditions and variables included in the model are: mold heat flux, roll positions and sizes, spray cooling tables, mapping positions of the spray cooling zones, spray nozzle layout (type, configuration and positioning relative to the support rolls and slab width), characterization of nozzle spray pattern, nozzle offset from the slab surface, slab dimensions and grade of steel. The model can be extended to virtually any slab or billet caster. Since each spray nozzle position and distribution is modeled, variations of the spray patterns with flow rate, and spray overlap can be simulated. Application of spray cooling water onto the narrow/edge face of the slab is implemented. This capability models spray cooling the slab narrow face from nozzles positioned outside of the slab width. Software interfaces are developed to enable users to easily setup, manage, run, and visualize the model output in a user-friendly GUI environment. Interfaces are included to directly export the heat transfer model results to the graphical visualization software *Tecplot* and to generate input files for stress analysis using the finite element analysis software *ABAQUS*. Examples of the results of the model are provided by comparing predicted temperatures to pyrometer measurements from 29 casting sequences for a 150 mm thick slab caster. Two demonstration cases are presented to show the importance of modeling narrow face spray cooling and its effect when casting variable slab widths.

INTRODUCTION

Continuously cast steel can contain defects, and the quality and material properties of the steel can be less than desired[1]. Defects encountered in continuous casting of steel include cracks, inclusions, macrosegregation, porosity and others[2-5]. Based on industrial data, it is estimated that a 1% reduction in scrapped production due to casting related defects (such as slab cracking from improper cooling) can result in annual energy savings of 0.14 trillion Btu (0.147 trillion kJ) for a typical steel mill[6]. Combining the scrap energy savings with optimized caster operations, such as the ability to direct hot charge steel slabs, a substantially larger energy savings can be achieved. Caster operation and practice are routinely determined to reduce casting defects by experience and empirical data. Computer modeling of the heat transfer and solidification of caster operating conditions provides a rational approach for designing casting processes. Through physics-based modeling, the thermal and solidification conditions which cause casting defects can be predicted and avoided. Furthermore, accurate heat transfer and solidification modeling is required to predict thermo-mechanical stress related defects, and macrosegregation and porosity defects. In addition to avoiding defects, modeling-based caster operating practices will optimize production, improve product quality, increase plant capacity and reduce production costs by improving caster operation.

Computer modeling in continuous casting is wide ranging[7,8]. Some computer models focus on the modeling of solidification and stresses in the mold or between a set of rolls[9,10]. The modeling effort presented here describes the caster heat transfer in as much detail as possible from the liquid meniscus to the cutoff torch. This work builds on earlier computer simulation models of continuous casters and a dynamic spray cooling control algorithm to optimize caster operation under transient conditions (e.g., casting speed changes)[11-13].

A key contribution of the model described here is its realistic definition of the secondary spray cooling conditions. Consequently, this modeling effort has benefitted from past work on the topic. The importance of secondary cooling spray and its physical complexity have been thoroughly reviewed[14]. The local heat extraction from the slab surface is determined and controlled primarily by the water spray flux (flow rate per unit area of slab surface). A number of sources of experimental measurements were consulted as possible heat transfer correlations between water spray flux and heat transfer coefficient to use in modeling[15-17]. From parametric studies, it has been found that the correlation of Nozaki et al. provides the best agreement between measured and predicted surface temperatures[15]. Clearly, parameters other than spray flux can influence the heat transfer due to secondary cooling spraying. The Nozaki correlation includes spray water and slab surface temperatures as parameters as well. Also hydraulic pressure affects the impact pressure of the spray on the slab surface, and

likewise the heat transfer. For high pressure water sprays, the reader is directed to the experimental work by Ito et al. who see a 2.8 times increase in heat transfer coefficient if the nozzle hydraulic pressure is increased from 0.7 to 5 MPa[18].

Assuming the spray pattern and distribution for a given spray nozzle on the caster is accurately known, the model presented here can be used to design spray layouts that improve slab quality through more uniform cooling. For example, El-Bealy has used heat transfer and solidification modeling to propose a criterion to evaluate the effectiveness of spray cooling in continuous steel casting and its impact on slab quality[19]. It is demonstrated that this "homogeneity degree of cooling pattern" HDCP criteria could be used to design an air-water mist nozzle spray pattern with more uniform cooling than traditional hydraulic or current air-water mist nozzles. The improved cooling reduces surface temperature fluctuations and is expected to improve quality both on the slab surface and inside the slab. It was recommended that plant trials be undertaken to demonstrate the improvement in quality by using the nozzle.

Presented here is a three-dimensional steady-state model covering the entire steel strand, approximately 20 meters long. The model simulates heat transfer in the mold, and the effects on slab temperatures due to all rolls and spray nozzles. It has been configured and validated for several caster configurations in previous work[11,12]. It is presented here configured for still another caster configuration and with new features such as modeling the spray water on the slab narrow face and the resulting variation in cooling with slab width. The model can be used to investigate caster operating parameters (e.g., adjustment of spray pattern, water flow rates, casting speed, etc.). Predicted and measured slab temperatures are compared. The model is used in an example case study to demonstrate its use to adjust spray cooling and avoid problematic casting conditions.

MODEL DESCRIPTION

The heat transfer and solidification simulation model presented here solves a steady-state energy equation. The calculation domain and coordinate system used is shown in Figure 1(a) for the slab region having axes directions x in thickness, y in width, and z in casting direction originating from the liquid meniscus. The domain extends from the meniscus to a user-selectable distance down the caster. In order to reduce computation time, symmetry at the centerline of the slab thickness can be assumed. Both top- and bottom-facing surfaces are modeled and their spray conditions independently defined. Heat conduction in the slab is computed in the thickness and width directions. Axial conduction is not included in this model, since studies have shown that the axial conduction term does not affect the results appreciably under normal operating conditions for steel slab casters[20]. Energy transport in the casting direction is advected only by the casting speed. The effects of convection in the liquid and solidifying mush are approximated using a thermal conductivity enhancement factor β. The thermal conductivity enhancement is especially important to account for fluid flow in the liquid sump in and near the mold. The energy equation for the conditions described above is

$$\left(\rho c_p\right) V_{cast} \frac{\partial T}{\partial z} = \frac{\partial}{\partial x}\left(k_{eff} \frac{\partial T}{\partial x}\right) + \frac{\partial}{\partial y}\left(k_{eff} \frac{\partial T}{\partial y}\right) + \Delta h \; V_{cast} \frac{\partial (\varepsilon \rho)}{\partial z} \tag{1}$$

where ρ, c_p, T, t, V_{cast}, k_{eff}, ε, and Δh are the density and specific heat (averaged based on the solid fraction during solidification), temperature, time, casting speed, thermal conductivity (enhanced in the liquid and mush, and averaged based on solid fraction during solidification), solid fraction, and latent heat, respectively. The product ρc_p and the effective thermal conductivity k_{eff} are defined as

$$\rho c_p = \varepsilon \rho_s c_{ps} + \left(1-\varepsilon\right) \rho_l c_{pl} \tag{2}$$

$$k_{eff} = \left[\varepsilon k_s + \left(1-\varepsilon\right) k_l\right]\left[1 + \beta\left(1-\varepsilon\right)^2\right] \tag{3}$$

where k is the thermal conductivity and the property subscripts s and l denote solid and liquid property values, respectively. The value used for the thermal conductivity enhancement factor β is 4, but can be changed if desired. Temperature dependent properties (i.e. ρ, c_p, k_{eff}, and ε as dependent on T) are defined using tables of values. In particular, the *IDS* steel solidification model developed by Miettinen et al. has been used to generate such properties for a given alloy chemistry, and software has been written to generate properties for the model using *IDS* output[21]. Temperature and solid fraction in each computational cell are determined through iterations between the energy equation (1) and the solid fraction-temperature curve defined as part of the alloy dataset. These are coupled using Newton-Raphson iterations to determine the solid fraction and temperature during solidification according to the local cooling conditions. The finite volume approach and a TDMA solver with ADI sweeping are used in the numerical solution of the discretized equations.

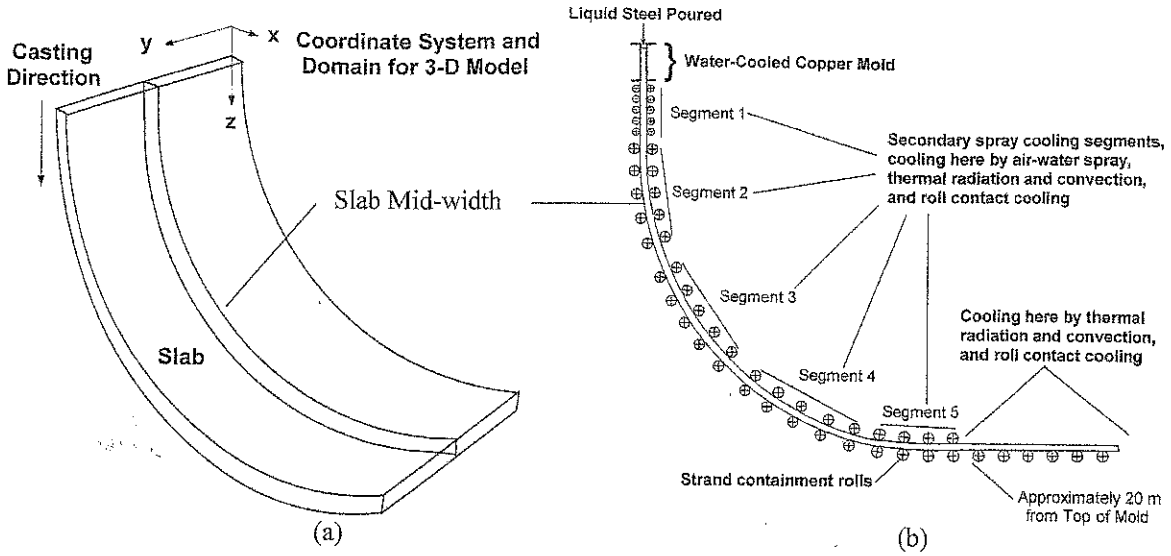

Figure 1. (a) Calculation domain and coordinate system used for the caster model. (b) Diagram of boundary conditions applied for an example caster layout with five segments of containment rolls on the slab mid-with plane.

Boundary Conditions and Model Features

Establishing proper boundary conditions for a continuous casting machine can be challenging due to the multiple modes of heat transfer involved and the many variables which are difficult to account for in the casting process. A diagram on the slab mid-width plane of boundary conditions applied for an example caster layout with five segments of containment rolls is shown in Figure 1b. Boundary conditions in the mold are determined from average mold heat flux measurements obtained from operating data at steady-state casting conditions. Data for the narrow and broad faces of the mold are collected separately. The average mold heat fluxes derived from the data for the narrow and broad faces are then correlated with dwell time in the mold. Dwell time is defined as mold length divided by casting speed. In the model, the user can select either a constant mold heat flux along the mold length, or a mold heat flux profile along the mold length corresponding to an average mold heat flux, or a prescribed mold heat flux profile along the mold length for the mold faces.

Spray cooling, natural convection, roller contact and radiation cooling boundary conditions are used in the model where applicable as shown in Figure 1b. Considerable effort has been made in the model to realistically model the secondary cooling sprays. By modeling each spray nozzle used in the caster (top and bottom surface) according to information provided by the caster operators, issues of spray non-uniformity and overlap can be investigated. The spray nozzle information included in the model are: the positions of the nozzles across (width direction) and along the strand (casting direction), the nozzle type, the fan angle and distribution of the spray flux from each nozzle, the height (offset) of the nozzle from the slab

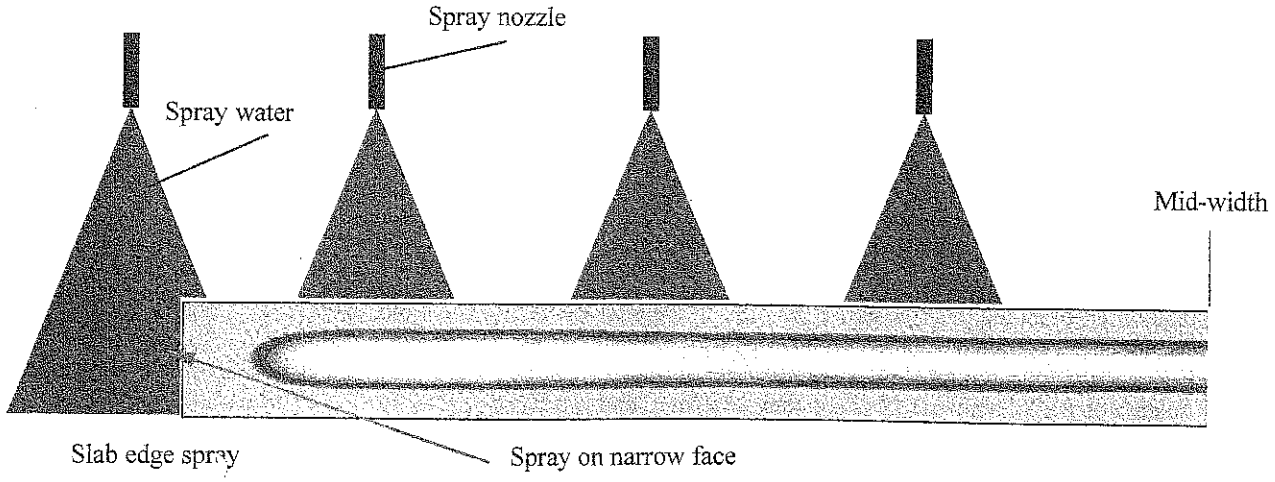

Figure 2. Diagram of spray cooling water applied to the narrow slab face from nozzles positioned outside of the slab width.

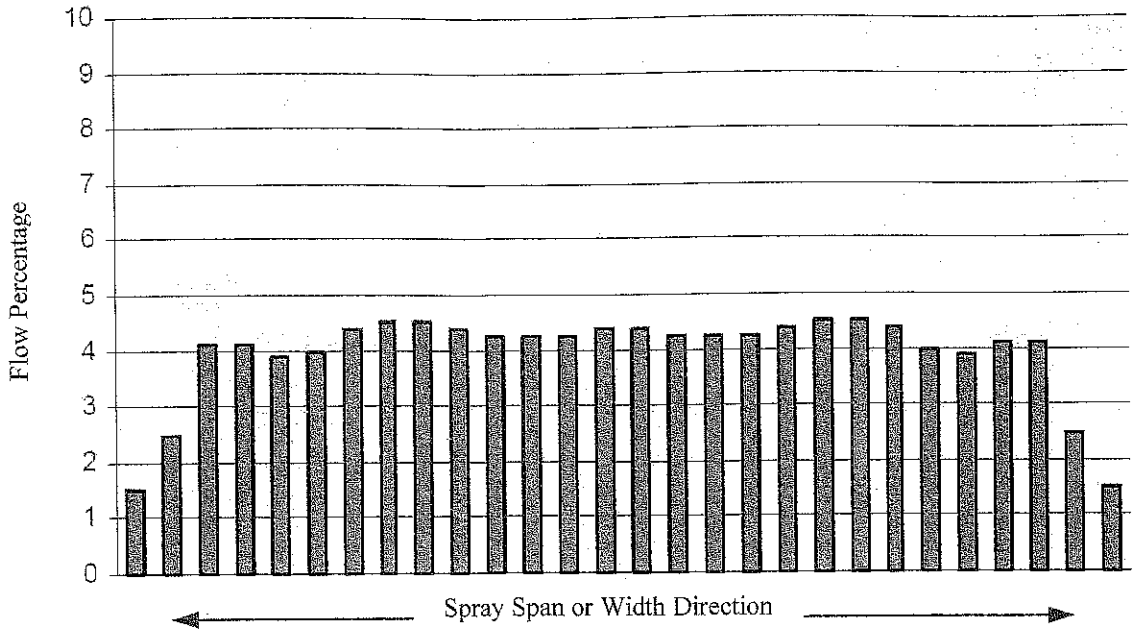

Figure 3. Spray flow/flux distribution from testing results across the span of a nozzle spraying at 45 psi (3.1 bar) air and 100 psi (6.9 bar) water at a 6 inch (152 mm) spray offset height from surface.

surface, and the spray water temperature. Application of spray cooling water onto the narrow/edge face of the slab is included in the heat transfer model. This capability was not developed in previous versions of the model[11,12]. As shown in Figure 2, this capability models spray cooling on the narrow slab face due to nozzles positioned outside of the slab width. Prior to this development, the model defined spray cooling on top and bottom facing surfaces only. Using this capability should predict more realistic temperatures at the slab corners. There are six different nozzle types defined in the model results presented here, as used in the actual caster. The span-wise spray flux distribution for each nozzle is uniquely defined as shown for example in Figure 3. Note that the distribution depends on the offset of the nozzle from the slab surface and other variables which are defined in the model configuration files. For the model results given here there are 415 nozzles used in the caster. The spray cooling curves defining how the spray water is apportioned to the machine segments (via secondary spray cooling loops or zones), and how spray water within a loop varies with casting speed, were provided by the caster operators and were defined in the model via configuration files. Currently there are ten spray cooling curves built into the model interface, but users can define their own, store them and load them for use. The secondary cooling spray heat transfer coefficients h_{spray} ($W/m^2/K$) used in the model are based on the correlation developed by Nozaki et al.

$$h_{spray} = 1570\, \dot{w}^{0.55} \left(1 - 0.15\ \cos\theta\right) \left(1\ - 0.0075\, (T_{spray} - 273.15)\right) / \alpha \qquad (4)$$

where $\dot{w}$ is the cooling water spray flux ($l/m^2/s$), θ is the slab surface angle from horizontal, T_{spray} is the temperature of the spray cooling water (K), and α is a machine dependent calibration factor (typically about 4)[15]. The model results presented here use an α of 4. The heat transfer coefficient varies locally according to the variables in Eq. 4 for each computational cell. If the slab surface cools below the Leidenfrost temperature, heat transfer is determined based on the work by Jacobi et al.[16]. Where there is no spray, natural convection heat transfer coefficients are used for upward facing, downward facing, vertical and inclined surfaces.

Thermal radiation is computed over the entire casting surface after the exit of the mold, except at roll contact points, using a radiative heat transfer coefficient in the exchange of heat with the caster environment temperature. Since the slab surface temperature is a variable in the radiative heat transfer coefficient, this boundary condition is iteratively determined in the solution. The environmental temperature is a model parameter, and is typically set to 34°C.

At the roll contact points, heat transfer occurs only between the slab and the roll. At the rolls, measurements have shown that temperature drops of over 200°C can occur, and heat transfer coefficients can be as high as 2500 ($W/m^2/K$)[17]. Here no such measurements have been made on the caster modeled. In lieu of such measurements, the effects of the individual roll contact

cooling are resolved using a constant roll heat transfer coefficient of 700 ($W/m^2/K$), and the environmental temperature (used for radiation exchange) is employed instead of the actual roll surface temperature, again due to lack of measurements. Although approximate, this combination of heat transfer boundary parameters at the rolls produces temperature drops at the roll contacts measured in the literature for similar casting machines.

The caster solidification model is composed several integrated modules in a graphical user interface package consisting of a preprocessor for setting up casting conditions (complete with property database and property visualization software modules), and a postprocessor to visualize temperature and solid fraction contours, and profiles, anywhere in the cast slab. The water spray flux on the top and bottom facing surfaces may also be visualized. An example of a spray flux plot from the postprocessor is seen in Figure 4. In addition, interfaces are included to directly export the heat transfer model results to the graphical visualization software Tecplot and to input files for stress analysis using the commercial finite element analysis software ABAQUS. Computation, steel property and solidification model setup screens from the models graphical user interface are shown in Figure 5.

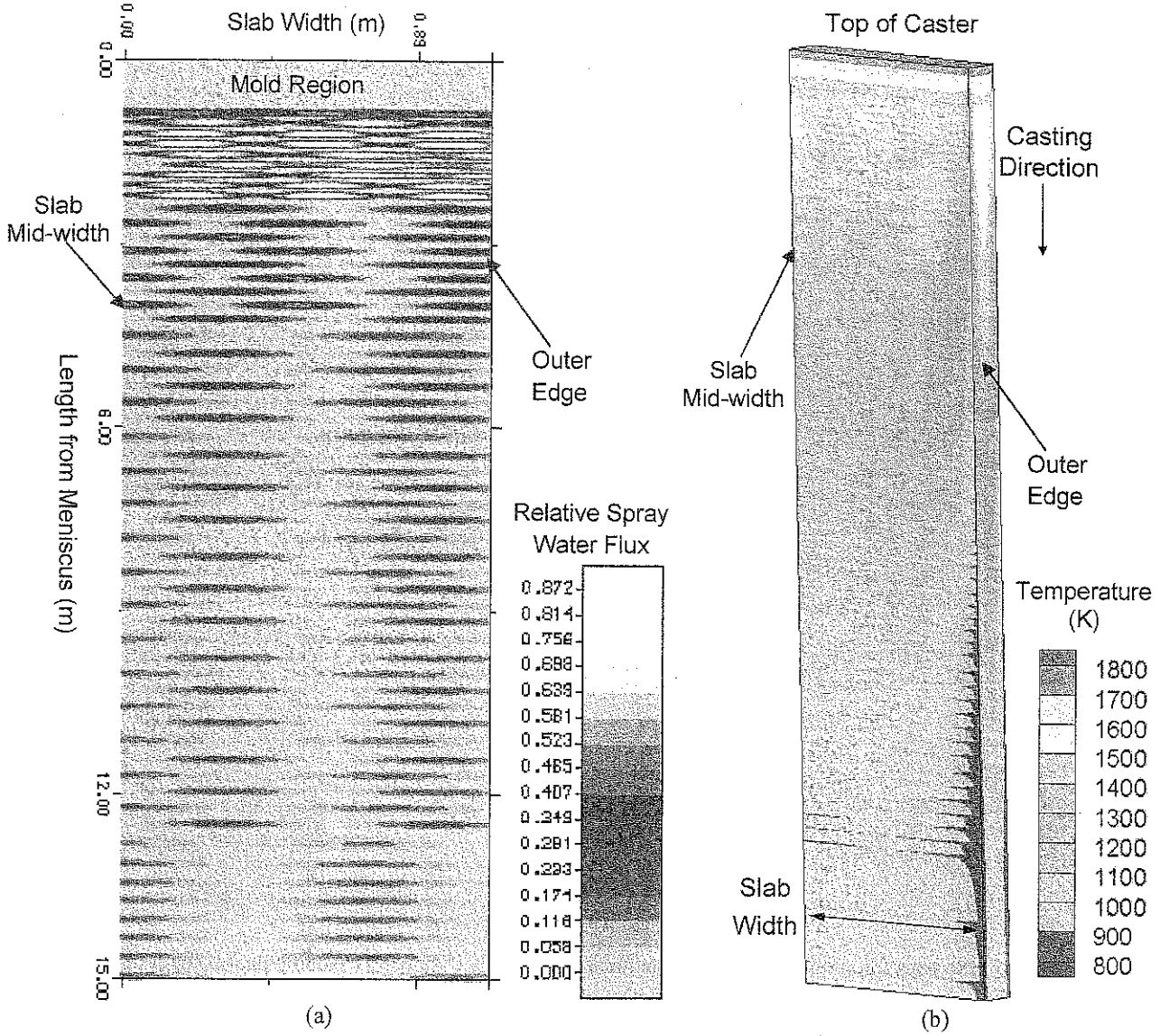

Figure 4. (a) Relative secondary spray cooling water flux (spray flux on surface divided by maximum spray flux) for half of slab width from 0 to 15 m from meniscus from the model post processor. Spray is symmetric about mid-width of slab. (b) Temperature results on the caster top-facing and outer edge surfaces for a domain of dimensions 0.15m thick x 2.2 m wide x 20 m long. Symmetry is assumed about the slab mid-width. Note the scaling differs in all directions.

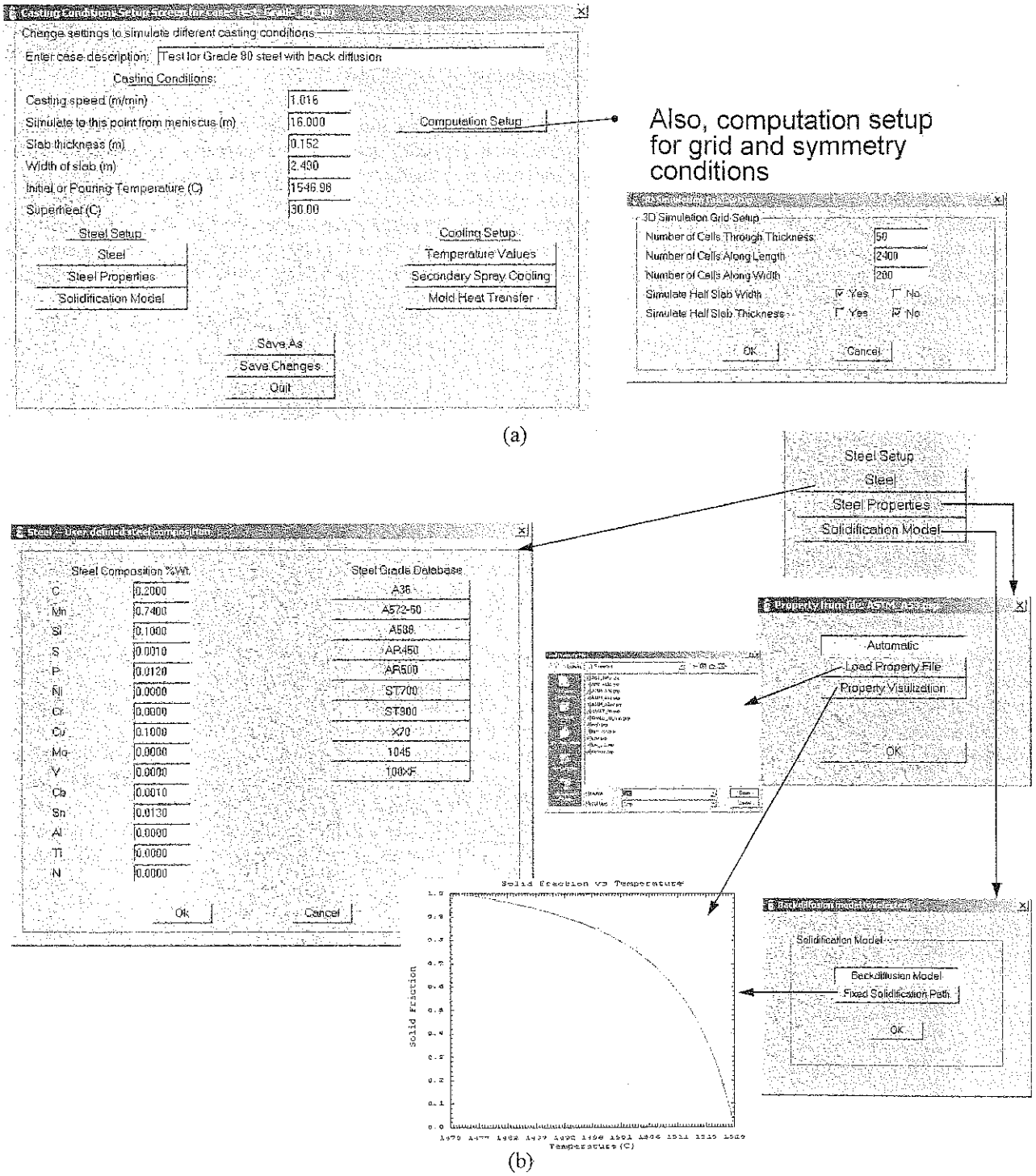

Figure 5. Example screens from the caster model graphical user interface showing (a) computation setup screen and (b) interface for setting steel properties and solidification modeling.

MODEL RESULTS

A plot of results for an example of relative spray flux on a slab surface from the model is shown in Figure 4a. This relative flux is the spray flux on surface (i.e. liter/minute/meter^2) divided by the maximum spray flux on the surface. The plot in Figure 4a is shown for half of the slab width. In this case, the spray is symmetric about the mid-width. The surface of the caster shown in this figure is from 0 to 15 m from meniscus. Note that higher fluxes are applied nearer the top of the caster, and that there is more spray overlap as well near the top of the caster.

An example temperature distribution result for a calculation domain of dimensions 0.15m thick x 2.2 m wide x 20 m long is shown in Figure 4b. The temperature results are shown on the caster top-facing and outer edge surfaces. Symmetry is assumed about the slab mid-width. Note that different scaling is used in the all directions.

The model was evaluated by comparing predicted temperatures with measured temperatures. Adjustments were made to the heat transfer correlation α factor used in the spray cooling calculations based on the model output until the best agreement between measured and predicted temperatures were obtained and the model was "calibrated". The temperature measurements were made by four pyrometers installed on the caster top-facing surface. Three were located at about half way down the caster (for example between segments 2 and 3 in our example caster shown in Figure 1b) and another was located further down the caster at roughly a location corresponding to between segments 4 and 5 for the example caster diagram. The pyrometers were located at various positions relative to the slab mid-width to provide a data for range of spray cooling conditions. Only measured temperatures for steady-state casting conditions (defined as online casting variables being constant for at least 20 minutes during a casting sequence) were compared with model results. Based on their variation with time, 95% confidence intervals were established for the temperature measurements. For the predicted temperatures, it was assumed the true positions of pyrometers on the caster had an uncertainty of ±4 cm about the positions provided by the caster operators. In this 8 cm square box the mean and confidence interval for the predicted temperature values were determined for the simulation values to provide a measure of uncertainty for the true sensor position.

From the online data collected over six weeks, 29 sets of steady-state data were used for the model calibration. After the model calibration, all 29 cases were run and a benchmark comparison was made between the measured and predicted temperatures. The comparison for one of the 29 cases is shown in Figure 6a with the uncertainties in measurements and predictions referenced above. Here the predicted temperature profiles along caster length and at the pyrometer temperature measurement locations are shown. Also in Figure 6a the temperature at the center mid-thickness of the slab is shown so the solidification end point may be visualized. Note that the solidification end point is not necessarily at the slab centerline/middle thickness point due to the realistic and non-uniform spray cooling in the model vis-à-vis the top- and bottom-facing surfaces. The comparison between measured and predicted temperatures for all 29 cases is presented in Figure 6b, where the dashed line corresponds to perfect agreement between them. Note that two pyrometer 3 measurements are circled, and these appear to be outliers where the temperature is under predicted significantly relative to the other data. Examining these cases, it was found that these slab widths are relatively narrow. The pyrometer location is close to the corner of the slab. At this location it is believed that the uncertainty in the pyrometer position relative to the slab corner should be eliminated if an accurate comparison is to be made. The predicted temperature variation near the slab corners is large.

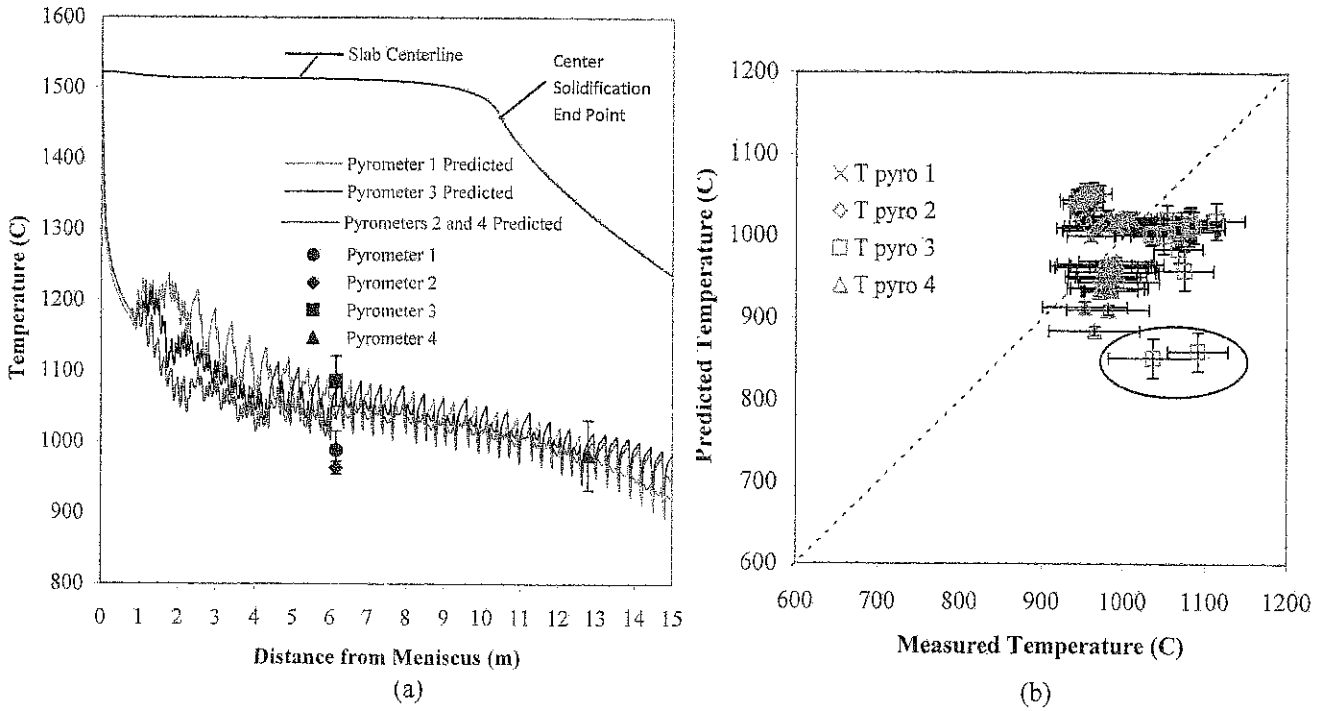

(a) (b)

Figure 6. (a) Predicted temperature profiles along caster length with measurements at the four pyrometer locations. Pyrometer error bars are 95% confidence intervals for the measurements from variations over time. (b) Predicted versus measured temperatures after model calibration.

Results for Cases Demonstrating Modeling of Slab Edge/Narrow Face Spray Cooling

Modeling the spray cooling water on the vertical narrow slab face as shown in Figure 2 has been found to provide new insights into the operation of the casting process. This spray is due to nozzles positioned outside of the slab width, and depending on the slab width, temperatures on the narrow face can vary significantly. At some slab widths the narrow face receives no spray cooling, while at other widths the narrow face is cooled substantially. The narrow face cooling conditions also influence the slab corners and can play a role in corner crack formation. In order to explore these effects, a test case comparing no edge spray effects (cooling by radiation and natural convection only) with edge spray included in the simulation is presented here. Plots of the narrow face temperature contours modeled without and with the narrow face spray mapping are given in Figure 7a and 7b, respectively, for a 0.15 m thick slab. When the narrow face spray mapping is used in the simulation, the narrow face as seen in Figure 7b is noticeably cooler and the temperature less uniform. The temperature is different by over 200°C at some locations compared to Figure 7a, and fluctuations around 100°C are observed. This case demonstrates the importance of including the effects of spray on the slab narrow face.

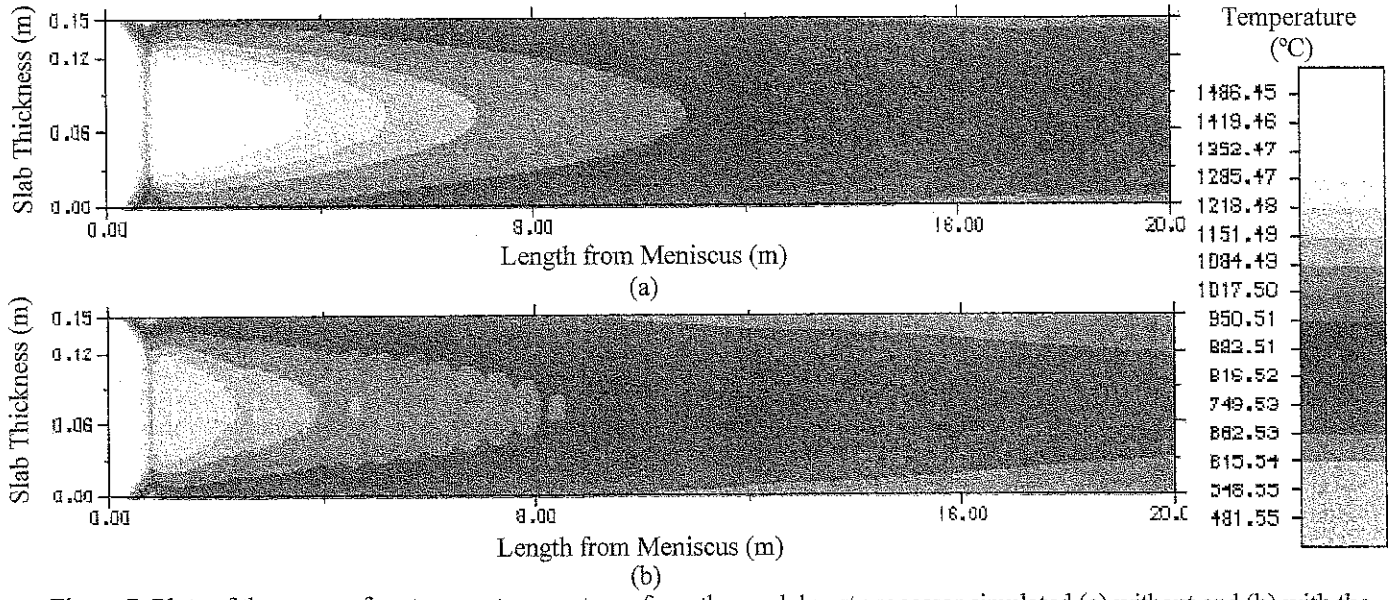

Figure 7. Plots of the narrow face temperature contours from the model post processor simulated (a) without and (b) with the narrow face spray mapping. With narrow face spray mapping, the narrow face is cooler and less uniform.

Next consider a second example application case study where three slab widths (73, 97 and 121 inches wide) are cast using the same spray cooling curve. In this case, the secondary cooling water is apportioned to cooling zones according to the same table depending on casting speed. Also, assume for this case that the caster operators cast at the same speed for all slab widths. The corner location of the three slab widths will cool differently for this case for the reasons discussed above due to differences in the slab edge position relative to the spray nozzles. The heat transfer model was run for this case using representative caster operating conditions for the three widths of interest.

The temperature profiles of the slab corners (temperature versus position from the top of the casting machine) were analyzed and averaged over the computational cells in the corner region of the slab. The averaging provides a less sensitive representation of the corner cooling conditions than the temperature of a given computational cell. The resulting temperature profiles of the three slab widths are shown in Figure 8a. Here it is assumed the steel has reduced ductility in the temperature range of 900°C to about 725°C. Considering the propensity for corner cracking of the slab in this temperature range during bending and unbending, this temperature range should be avoided in those regions of the caster. These temperature ranges and locations along the caster length are indicated in the plots in Figure 8. The model results in Figure 8a show that the corners of the 73 and 97 inch wide slabs are in the range where low ductility occurs during bending, whereas the corners of the 121 inch slab clearly avoid the problematic temperature range during both bending and unbending. Certainly a steel grade's ductility trough depends on steel chemistry and metallurgical factors, but the exact range is not critical for this demonstration case study.

Based on the results in Figure 8a the model demonstrates that the cooling should be modified according to the slab width cast. Using the model a new spray cooling curve (distributing water to the secondary cooling zones as a function of casting speed) was determined which avoids the ductility trough temperature range for this example. The temperature profiles

resulting for the newly developed spray cooling curve to be used for the 73 and 97 inch wide slabs are shown in Figure 8b and are compared to the wider slab cast with the original spray curve. This case study demonstrates the importance of modeling the edge spray again, and how the model can be used to evaluate current casting practices and guide changes to practices. Often caster operating practice uses the same spray cooling table/conditions regardless of slab width. This study demonstrates that practice should be reconsidered.

CONCLUSION

The continuous steel casting process can be improved through computer modeling by predicting the cause of casting defects and optimizing caster operating conditions. The heat transfer and solidification model presented here includes realistic features such as the mapping of individual spray nozzles and detailed boundary conditions. The model has been configured to reflect the casting conditions and practices for an operating caster. These conditions and practices are: mold heat flux data, roll positions and sizes, spray cooling tables (water flow rates as a function of casting speed for the spray cooling zones), mapping the positions of the spray cooling zones, spray nozzle layout (type, configuration and positioning relative to the support rolls and slab width), characterization of nozzle spray pattern, nozzle offset from the slab surface, and slab dimensions and grades of steel. The entire caster configuration can be modified using configuration files. The heat transfer model was validated and calibrated using temperature data measured by online pyrometers and mold heat flux data. The model presented here gives good agreement between measured and predicted temperatures. A user friendly software suite was developed to provide pre- and post-processing of the heat transfer model. This graphical user interface makes the model beneficial to users with a wide variation of technical expertise, ranging from plant operators to research engineers. The importance of modeling the slab edge/narrow face spray conditions is demonstrated. Increased temperature non-uniformity on the slab narrow face is predicted by its addition to the model. In addition, more realistic predictions of slab corner temperatures with varying slab widths are implemented by including the effects of spray cooling on the narrow slab face.

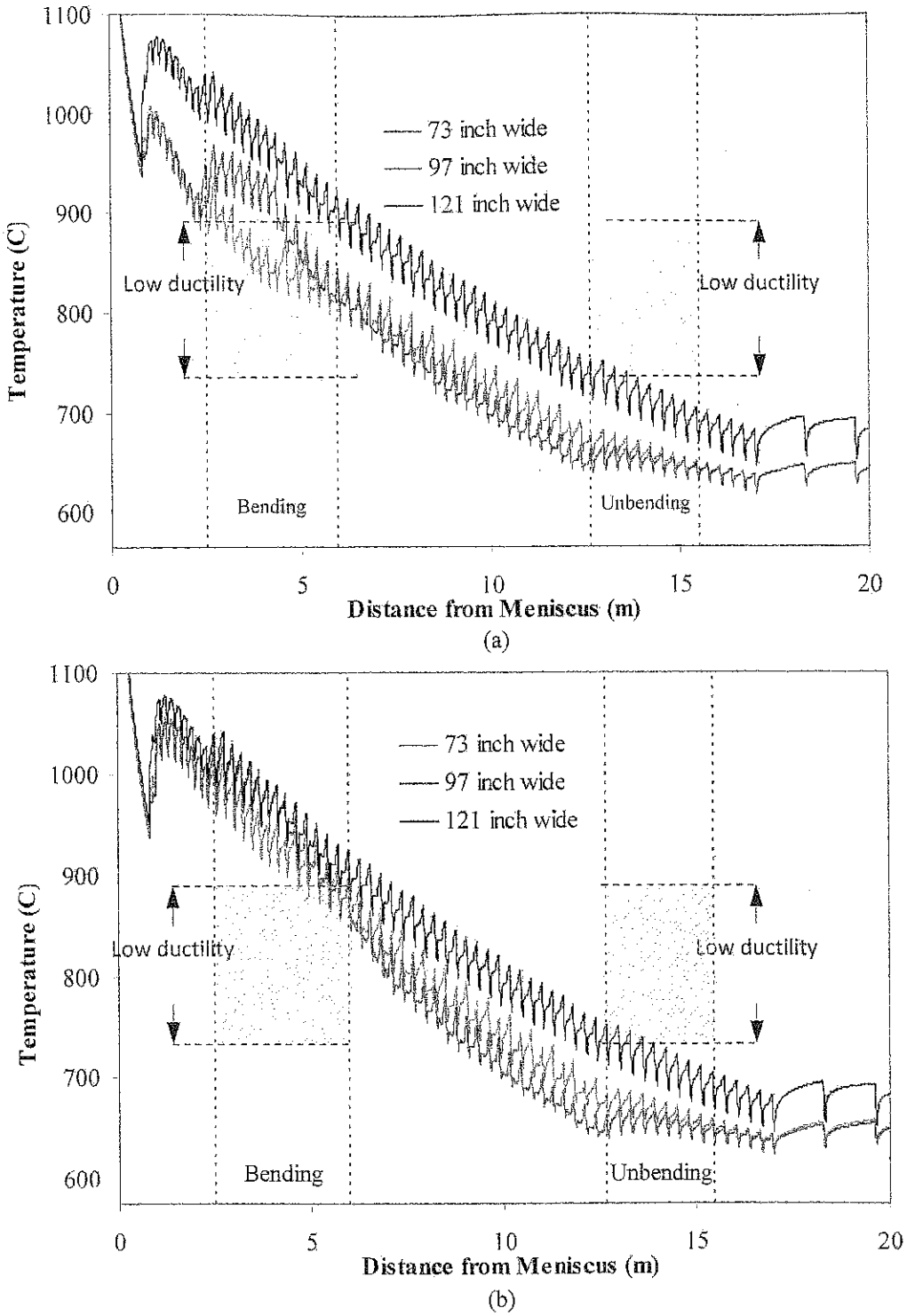

Figure 8. Temperature profiles along caster length at slab corners for three slab widths using (a) the same cooling curve for all slab widths and (b) a modified cooling curve which avoids corner temperatures in the ductility trough for the 97 and 73 inch wide slabs. Bending and unbending locations are indicated along with the example low ductility temperature range.

ACKNOWLEDGMENTS

This work was conducted through funding from the Iowa Energy Center under grant number 09-02. The authors gratefully acknowledge this support. In addition, the authors thank SSAB for their participation in the project, guidance and temperature data for model calibration and validation.

REFERENCES

1. J.K. Brimacombe, "The Challenge of Quality in Continuous Casting Processes," *Metall. Mater. Trans. A*, Vol. 30A, 1999, pp. 1899-1912.
2. J.K. Brimacombe and K. Sorimachi, "Crack Formation in the Continuous Casting of Steel," *Metall. Mater. Trans. B*, Vol. 8B, 1977, pp. 489-505.
3. L. Zhang and B.G. Thomas, "Inclusions in Continuous Casting of Steel," *XXIV National Steelmaking Symposium*, November 26-28, 2003, pp. 138-183.
4. C. Beckermann, "Modelling of Macrosegregation: Applications and Future Needs," *Int. Mater. Rev.*, Vol. 47, 2002, pp. 243-261.
5. W.R. Irving, "Continuous Casting of Steel, London," UK: Inst. of Materials, 1 Carlton House Terrace, 1993, pp. 93-155.
6. American Iron and Steel Institute, "Saving One Barrel of Oil per Ton: A New Roadmap for Transformation of Steelmaking Process," available at http://www.steel.org/, October 2005.
7. B.G. Thomas, "Modeling of the Continuous Casting of Steel: Past, Present and Future," 59th Electric Furnace Conference Proceedings, ISS, Warrendale, PA, 2001, pp. 3-30.
8. B.G. Thomas, "Recent Advances in Computational Modeling of Continuous Casting of Steel," Scanmet II Conference, MEFOS, Vol. 1, 2004, pp. 243-252.
9. S. Koric, L. Hibbeler, and B.G. Thomas, B.G., "Explicit Coupled Thermo-Mechanical Finite Element Model of Steel Solidification," *Int. J. Num. Meths. Engineering*, Vol. 78, 2009, pp. 1-31.
10. S.J. Camporredondo, E.A. Castillejos, G.F. Acosta, M.E. Gutierrez, and G.M. Herrera, "Analysis of Thin-slab Casting by the Compact-strip Process: Part II. Effect of Operating and Design Parameters on Solidification and Bulging," *Metall. Mater. Trans. B*, Vol. 35, No. 3, 2004, pp. 561-573.
11. R.A. Hardin, H. Shen, and C. Beckermann, "Heat Transfer Modeling of Continuous Steel Slab Casters Using Realistic Spray Patterns," in *Modeling of Casting, Welding and Advanced Solidification Processes IX*, eds. P.R. Sahm et al., Shaker Verlag, Aachen, Germany, 2000, pp. 729-736.
12. H.F Shen, R.A. Hardin, R. MacKenzie, and C. Beckermann, "Simulation using Realistic Spray Cooling for the Continuous Casting of Multi-Component Steel," *J. Materials Science and Technology*, Vol. 18, 2002, pp. 311-314.
13. R.A. Hardin, K. Liu, A. Kapoor, and C. Beckermann, "A Transient Simulation and Dynamic Spray Cooling Control Model for Continuous Steel Casting," *Metall. Mater. Trans. B*, Vol. 34B, 2003, pp. 297-306.
14. J. Sengupta. B.G. Thomas and M.A. Wells, "The Use of Water Cooling during the Continuous Casting of Steel and Aluminum Alloys," *Metall. Mater. Trans. A*, Vol. 36A, 2005, pp. 187-204.
15. T. Nozaki, J. Matsuno, K. Murata, H. Ooi and Kodama, "A Secondary Cooling Pattern for Preventing Surface Cracks of Continuous Casting Slab," *Trans. ISIJ*, vol. 18, 1978, pp. 330-338.
16. H. Jacobi, G. Kaestle and K. Wünnenberg, "Heat Transfer in Cyclic Secondary Cooling during Solidification of Steel," *Ironmaking and Steelmaking*, Vol. 11, No. 3, 1984, pp. 132-145.
17. M. El-Bealy, N. Leskinen and H. Fredriksson, "Simulations of Cooling Conditions in Secondary Cooling Zones in Continuous Casting Process," *Ironmaking and Steelmaking*, Vol. 22, No. 3, 1995, pp. 246-255.
18. Y. Ito, T. Murai, Y. Miki, M. Mitsuzono, and T. Goto, "Development of Hard Secondary Cooling by High-pressure Water Spray in Continuous Casting," *ISIJ International*, Vol. 51, No. 9, 2011, pp. 1454-1460.
19. M.O. El-Bealy, "Air-Water Mist and Homogeneity Degree of Spray Cooling Zones for Improving Quality in Continuous Casting of Steel," *Steel Research International*, Vol. 82, No. 10, 2011, pp. 1187-1296.
20. R. A. Hardin, K. Liu and C. Beckermann, "Development of a Model for Transient Simulation and Control of a Continuous Slab Caster," in *Materials Processing in the Computer Age III*, eds. V.R. Voller and H. Henein, TMS, Warrendale, PA, 2000, pp. 61-74.
21. J. Miettinen, S. Louhenkilpi, H. Kytönen, and J. Laine, "IDS: Thermodynamic-kinetic-empirical tool for modelling of solidification, microstructure and material properties," *Math. Comput. Simul.*, Vol. 80, No. 7, 2010, pp. 1536-1550.

PROCEEDINGS OF THE 2ND INTERNATIONAL SYMPOSIUM ON THE RECENT DEVELOPMENTS IN PLATE STEELS

3–6 JUNE 2018 | ORLANDO, FLA., USA

A Publication of the Association for Iron & Steel Technology

2018
2nd International Symposium on the Recent Developments in Plate Steels
Proceedings

ISBN: 978-1-935117-74-2 (Print)
978-1-935117-75-9 (Digital)

Association for Iron & Steel Technology
186 Thorn Hill Road
Warrendale, PA 15086-7528
USA
Phone: +1.724.814.3000
Fax: +1.724.814.3001
memberservices@aist.org
AIST.org